PROCEEDINGS OF SPIE

SPIEDigitalLibrary.org/conference-proceedings-of-spie

Super-nonlinear fluorescence microscopy for high-contrast deep tissue imaging

Lu Wei, Xinxin Zhu, Zhixing Chen, Wei Min

Lu Wei, Xinxin Zhu, Zhixing Chen, Wei Min, "Super-nonlinear fluorescence microscopy for high-contrast deep tissue imaging," Proc. SPIE 8948, Multiphoton Microscopy in the Biomedical Sciences XIV, 894825 (28 February 2014); doi: 10.1117/12.2038753

SPIE.

Event: SPIE BiOS, 2014, San Francisco, California, United States

Super-nonlinear fluorescence microscopy for high-contrast deep tissue imaging

Lu Wei[a]; Xinxin Zhu[a]; Zhixing Chen[a]; Wei Min[a,b]
[a]Department of Chemistry, Columbia University, New York, NY 10027
[b]Kavli Institute for Brain Science, Columbia University, New York, NY 10027

Abstract

Two-photon excited fluorescence microscopy (TPFM) offers the highest penetration depth with subcellular resolution in light microscopy, due to its unique advantage of nonlinear excitation. However, a fundamental imaging-depth limit, accompanied by a vanishing signal-to-background contrast, still exists for TPFM when imaging deep into scattering samples. Formally, the focusing depth, at which the in-focus signal and the out-of-focus background are equal to each other, is defined as the fundamental imaging-depth limit. To go beyond this imaging-depth limit of TPFM, we report a new class of super-nonlinear fluorescence microscopy for high-contrast deep tissue imaging, including multiphoton activation and imaging (MPAI) harnessing novel photo-activatable fluorophores, stimulated emission reduced fluorescence (SERF) microscopy by adding a weak laser beam for stimulated emission, and two-photon induced focal saturation imaging with preferential depletion of ground-state fluorophores at focus. The resulting image contrasts all exhibit a higher-order (third- or fourth- order) nonlinear signal dependence on laser intensity than that in the standard TPFM. Both the physical principles and the imaging demonstrations will be provided for each super-nonlinear microscopy. In all these techniques, the created super-nonlinearity significantly enhances the imaging contrast and concurrently extends the imaging depth-limit of TPFM. Conceptually different from conventional multiphoton processes mediated by virtual states, our strategy constitutes a new class of fluorescence microscopy where high-order nonlinearity is mediated by real population transfer.

Keywords: Nonlinear microscopy, multiphoton microscopy, imaging-depth limit, real population transfer, deep-tissue imaging

1. INTRODUCTION

Optical microscopy has revolutionized the way biological structures and functions are studied on microscopic scales. In particular, the invention of fluorescence microcopy together with the continuous development of versatile fluorophores, has allowed the visualization of molecules of interest in biological systems with superb specificity and sensitivity. Among all fluorescence imaging modalities, two-photon fluorescence microscopy (TPFM) offers the deepest imaging penetration depth, thanks to its nonlinear excitation scheme in which the excited fluorescence is mostly generated from the laser focus [1]. This spatially confined excitation thus allows the direct detection by a large-area non-descanned detector without the use of pinholes. Such avoidance of using pinholes drastically enhances the fluorescence detection sensitivity of TPFM in scattering tissues, thus makes TPFM a particularly suitable optical microscopy technique of imaging into turbid samples.

However, there still exits a fundamental imaging-depth limit for TPFM [2, 3]. Such an imaging-depth limit arises because the optical sectioning ability of two-photon fluorescence being generated only within the focal volume no longer holds when imaging deep enough into

Multiphoton Microscopy in the Biomedical Sciences XIV, edited by Ammasi Periasamy, Peter T. C. So, Karsten König, Proc. of SPIE Vol. 8948, 894825 · © 2014 SPIE
CCC code: 1605-7422/14/$18 · doi: 10.1117/12.2038753

scattering samples. Beyond a certain depth, the laser power deposited on the out-of-focus layer becomes so high that the fluorescence from out-of-focus fluorophores (especially those located near the sample surface) begins to even dominate the detected signal from the desired focal volume, as illustrated by the fluorescent beads images in Fig. 1. Obviously, this image-contrast determined imaging-depth limit could not be overcome by further increasing the laser power which would promote signal and background equally. For mouse brain tissues expressing GFP, the corresponding depth limit has been experimentally determined to be about 1 mm [2], which covers only a fraction of the thickness of the mammalian brain.

Formally, the focusing depth, at which the in-focus signal and the out-of-focus background are equal to each other, is defined as the fundamental imaging-depth limit [2, 3], shown as in Eq. (1):

$$\left(\frac{S}{B}\right)_{2P} = \frac{\int_{V_{in}} \int_0^{\tau} C_S(r,z) I^2(r,z,t)\, dt\, dV}{\int_{V_{out}} \int_0^{\tau} C_B(r,z) I^2(r,z,t)\, dt\, dV} = 1 \qquad (1)$$

where V_{in} is the focal volume, V_{out} is the total sample volume along the light path but excluding the focal volume, r is the distance from the optical axis, z is the axial distance from the tissue surface, C is the local fluorophore concentration, I is the local imaging laser intensity, and τ is the pixel dwell time during imaging. Eq. (1) assumes no fluorophore saturation or photobleaching and that the fluorescence collection efficiencies at the wide-field detector are nearly identical for the signal and the background [3].

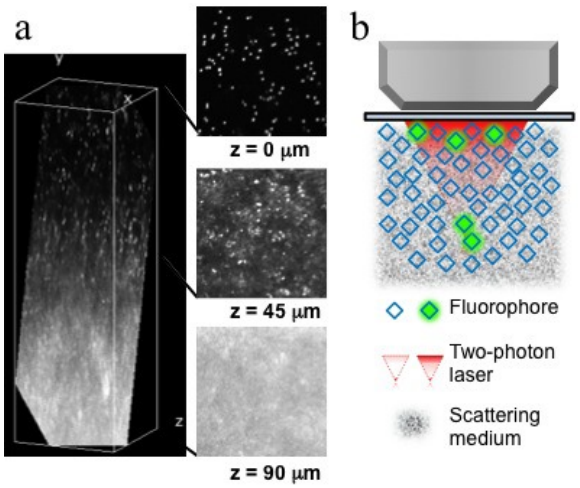

Fig. 1 Fundamental imaging-depth limit of two-photon fluorescence microscopy (TPFM). (a) TPFM imaging of fluorescent beads embedded in a turbid phantom tissue sample. With increasing imaging depth, the excitation laser power is also elevated to maintain a nearly constant detectable fluorescence signal from the focal plane. Due to the contribution from the out-of-focus excitation, the obtainable image contrast is deteriorating when the focal depth is increasing from 0 μm to 45 μm, and to 90 μm. (b) Cartoon illustration of the signal-to-background limited fundamental imaging-depth limit of TPFM at which the in-focus signal and the out-of-focus background become comparable.

Motivated by performing high-contrast high-resolution optical imaging inside living tissues and organisms, extensive efforts have been made along the direction of reducing light scattering

inside biological samples. Notable techniques include adaptive optics [4, 5], imaging with structued illumination [6], longer excitation wavelengths [7], optical phase conjugation [8], differential abberation imaging [9] and focal modulation [10]. Note that relatively few work has been reported along the direction of exploring new spectroscopic transitions of the targeted fluorophores.

Herein, we introduce a novel strategy of performing super-nonlinear microscopy to tackle this image-depth limit. Our methods are based on the premise that higher-order (more than second-order) nonlinearity on the laser intensity dependence should provide superior discrimination mechanism against the out-of-focus background when comparing to the standard TPFM. Quantitatively, our strategy is justified by the fact that, when the depth limit is reached as defined in Eq. (1), $I^2(r,z)$ at the focus is much more intense than its out-of-focus counterpart, since the number of out-of-focus fluorophores is almost always orders-of-magnitude larger than that of the in-focus ones. As a result, the extra nonlinear processes will preferentially occur inside the focal volume where the excitation intensity is the highest, providing additional spatial confinement (i.e., signal-to-background contrast) on top of the standard two-photon excitation.

Technically, we will discuss three distinct super-nonlinear approaches, namely, multiphoton activation and imaging (MPAI) harnessing novel photo-activatable fluorophores [11-13], stimulated emission reduced fluorescence (SERF) microscopy with an extra weak stimulated emission (S.E.) beam [14, 15], and two-photon induced focal saturation imaging with ground-state depletion of fluorophores [16]. Both the physical principles and the imaging demonstrations will be provided for each super-nonlinear microscopy technique.

2. MULTIPHOTON ACTIVATION AND IMAGING (MPAI) — Utilizing novel photo-activatable fluorophores

MPAI utilizes photo-activatable fluorophores (PAFs) to extend the fundamental imaging-depth limit, with fourth-order fluorescence-to-intensity dependence [11]. Unlike traditional fluorophores that always remain in their bright states, PAFs start with dark states, and permit photo-induced transitions from dark states to bright states. MPAI, containing two subsequent steps, first preferentially activates the PAFs at focus to bright states while remain most PAFs out of focus at dark states, and then images the activated PAFs (Fig. 2a) with much improved signal-to-background image contrast.

We now briefly discuss the improved S/B achievable by MPAI. $C(r,z)$ in Eq. (1) should be replaced by $A(r,z,t)$, the activated concentration of the PAFs in the bright state that is ready to fluoresce upon excitation. Quantitatively, $A(r,z,t)$ is the product of $C(r,z)$ and the time-dependent two-photon activation yield, $\eta(t)$:

$$A(r,z,t) = C(r,z)\eta(r,z,t) \tag{2}$$

In the simplest condition, $\eta(t)$ follows a first-order chemical kinetics:

$$\eta(t) = 1 - \exp\left[-\sigma I_a^2(r,z,t)t\right],\ 0 \le t \le \tau \tag{3}$$

The rate constant is proportional to $I_a^2(r,z)$ of the activation laser and the two-photon activation cross section, σ. With a non-saturating activation yield of $\eta(t)$, the signal-to-background ratio for PAFs can thus be expressed as:

$$\left(\frac{S}{B}\right)_{PAFs} \approx \frac{\int_{V_{in}}\int_0^{\tau} C_S(r,z)I_a^2(r,z,t)I^2(r,z,t)\,dt\,dV}{\int_{V_{out}}\int_0^{\tau} C_B(r,z)I_a^2(r,z,t)I^2(r,z,t)\,dt\,dV} \tag{4}$$

which exhibits an overall fourth-order nonlinear dependence on the excitation laser intensity. A related technique of multiphoton deactivation and imaging (MPDI) using photo-switchable fluorophores could lead to a similar depth extension [12, 13].

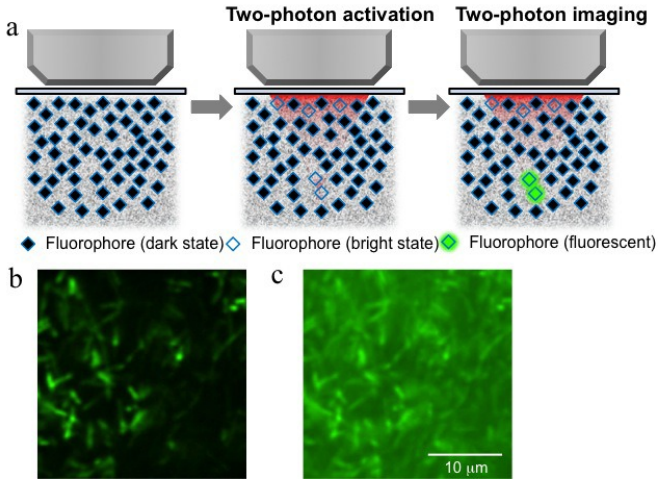

Fig. 2. Multiphoton activation and imaging (MPAI). (a) Cartoon demonstration of MPAI procedure. When imaging with PAFs which are originally in the dark state, the two-photon activation switch on a higher percentage of PAFs at focus than those out-of-focus. Such a spatial disparity of dark-bright transitions leads to a significantly decreased background fluorescence in the subsequent imaging. (b-c) Deep tissue imaging comparison (MPAI versus the regular TPFM) for 3D turbid samples made of *E. coli* cells expressing photoactivatable-GFP (pa-GFP), embedded in 2% agarose gel. At a 100 μm depth inside the turbid gel sample, MPAI with pa-GFP offers a satisfactory image contrast (b), while for TPFM, the out-of-focus background is overwhelming when the same sample with all the pa-GFP being activated to become regular GFP (c).

As demonstrated in 3D turbid samples made of *E. coli* cells expressing photoactivatable-GFP (pa-GFP) embedded in 2% agarose gel, MPAI with pa-GFP offers a significantly improved image contrast (Fig. 2b) when comparing to the standard TPFM image on regular GFP (all the pa-GFP being activated) of the same depth on the same sample (Fig. 2c). Hence, MPAI preferentially suppresses the bright state fluorophore number out of focus to significantly reduce the undesired background contribution, effectively extending the fundamental imaging-depth limit of the standard TPFM.

3. STIMULATED EMISSION REDUCED FLUORESCENCE (SERF) MICROSCOPY — Adding a weak modulated stimulated emission laser

SERF, with an additional weak laser beam to induce stimulated emission (i.e., to compete with fluorescence emission) of the excited fluorophores preferentially within the focal volume, displays a third-order signal dependence on excitation intensity, extending the fundamental imaging-depth limit by up to 1.8 times [14, 15]. In SERF, we adopt a scheme that combines an intensity-modulated continuous wave (CW) S.E. beam collinearly with a standard pulsed two-photon excitation laser beam and then detects the reduced fluorescence signal, which occurs primarily inside focal volume (Fig. 3 a, b, c).

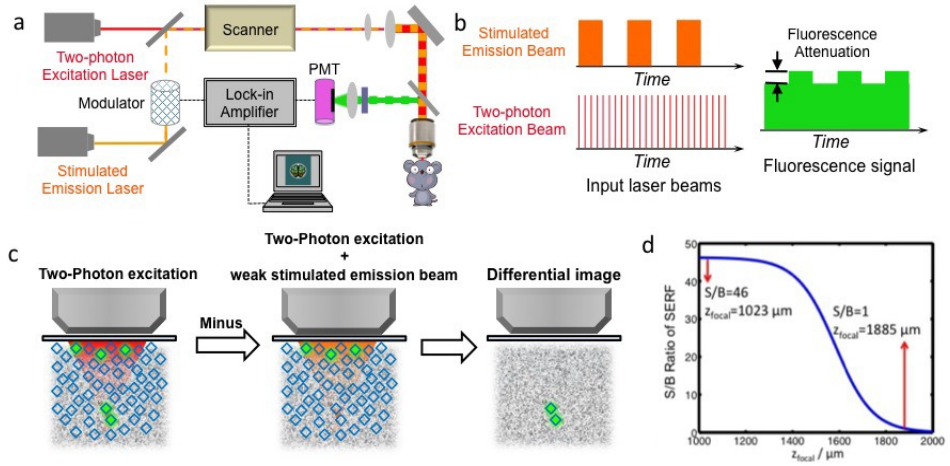

Fig.3. Stimulated emission reduced fluorescence (SERF) microscopy. (a) Microscopy setup. (b) Illustration of combining an intensity modulated stimulated emission (S.E.) beam with a pulsed two-photon beam, and detects the fluorescence attenuation signal. (c) Cartoon demonstration of SERF in which the reduced fluorescence is mainly occurring inside the focal volume. (d) Numerical simulation result using typical parameters for brain tissues shows that SERF could extend the fundamental depth limit from 1023 μm of TPFM to the new 1885 μm (where S/B approaches unit), with 1.8 times depth extension.

Analytically, two-photon fluorescence emission rate (R) of a single fluorescent molecule and its counterpart in the presence of S.E. attenuation (R'):

$$R = f_{rep} k_{exc} \tau_{pulse} \eta \tag{5}$$

$$R' = f_{rep} k_{exc} \tau_{pulse} \eta' = f_{rep} k_{exc} \tau_{pulse} \eta \frac{k_{fl}}{k_{fl} + k_{S.E.}} \tag{6}$$

where f_{rep} is the repetition rate of the excitation pulse train, τ_{pulse} is the pulse width (~100 *fs* for a typical 2P laser), η is the fluorescence quantum yield, and η' is effective fluorescence quantum yield in the presence of the S.E. beam. $k_{fl} = 1/\tau_{fl}$ where τ_{fl} is the fluorescence lifetime. $k_{S.E.} = \sigma_{S.E.} I_{S.E.} \lambda_{S.E.} / hc$ is the S.E. rate where $\sigma_{S.E.}$ is the S.E. cross-section of the molecule at

$\lambda_{S.E.}$. Subtracting Eq. (6) from Eq. (5), we thus obtain the fluorescence attenuation rate (defined as R_{SERF}) as:

$$R_{SERF} \equiv R - R' = f_{rep} k_{exc} \tau_{exc} \eta \frac{k_{S.E.}}{k_{fl} + k_{S.E.}} \tag{7}$$

When $I_{S.E.}$ is weak so that $k_{S.E.} << k_{fl}$, the S/B of SERF is thus:

$$\left(\frac{S}{B}\right)_{SERF} \approx \frac{\int_{V_{in}} \int_0^{\tau} C_S(r,z) I_{S.E.}(r,z) I_{exc}^2(r,z,t)\, dt\, dV}{\int_{V_{out}} \int_0^{\tau} C_B(r,z) I_{S.E.}(r,z) I_{exc}^2(r,z,t)\, dt\, dV} \tag{8}$$

exhibiting an overall third-order nonlinearity (second order from the excitation laser and extra linear from the stimulated emission laser). Our numerical simulation [14] further reveals that SERF could extend the fundamental imaging-depth limit of TPFM by 1.8 times (Fig. 3d).

4. TWO-PHOTON INDUCED FOCAL SATURATION IMAGING — By ground-state fluorophore depletion at focus

Two-photon induced focal saturation imaging utilizes the fact that, at the fundamental image-depth limit of the standard TEFM, the laser intensity at the focus is much higher than the intensity out of focus. Thus, a relatively high power of the pulsed two-photon excitation laser could weakly deplete the ground-state fluorophores at the focus (Fig. 4a). By sequentially acquiring a low power image without excitation saturation and a high power image with weak focal excitation saturation, the subsequent differential image displays a fourth-order signal dependence on the excitation intensity (Fig. 4b), offering high contrast deep tissue imaging (16).

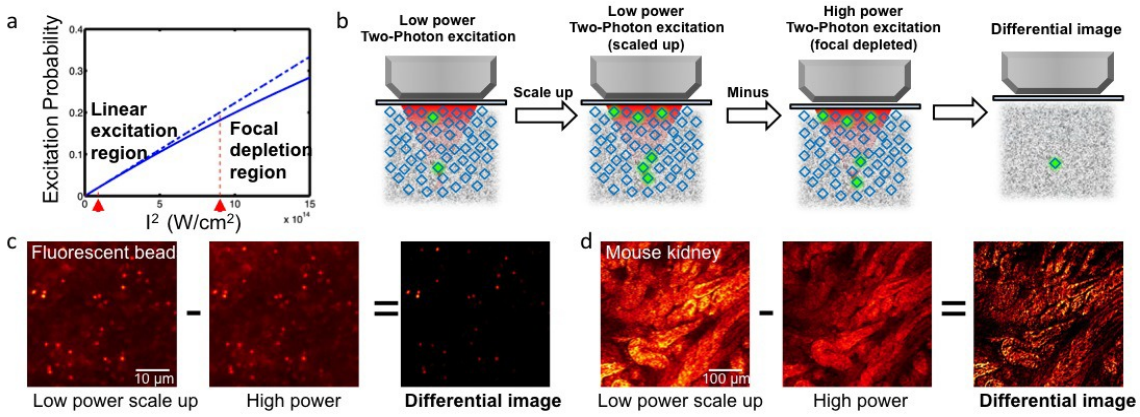

Fig.4. Two-photon induced focal saturation imaging. (a) Principle of using excitation saturation at focus and linear excitation out of focus. (b) Cartoon illustration of focal saturation imaging scheme. (c) Demonstration using fluorescent beads embedded in 3D turbid gels. The differential image between a scale-upped low power excited image and a high power focal saturated image displays a resulting fluorescent bead image with much increased contrast than the original. (d) Demonstration on mouse kidney tissues by detecting two-photon excited auto-fluorescence.

The two-photon excitation probability of a single fluorophore after each pulse is $P = 1 - \exp\left[-\sigma_{exc} I^2(r,z,t)\tau_{pulse}\right]$, where σ_{exc} is the two-photon cross section. A low power unsaturated image is first acquired, which can be digitally scaled up according to $I^2_{high}(r,z,t) = NI^2_{low}(r,z,t)$, where N is the scaling constant. At the weakly saturation region, $P \approx \sigma_{exc}(I^2(r,z,t) - I^4(r,z,t)/2)\tau_{pulse}$. The consequent differential signal between the above two will exhibit a corresponding S/B contrast as:

$$\left(\frac{S}{B}\right)_{Focal Saturation} = \frac{\int_{V_{in}} \int_0^{\tau} C_S(r,z) I^4_{high}(r,z,t)\, dt\, dV}{\int_{V_{out}} \int_0^{\tau} C_B(r,z) I^4_{high}(r,z,t)\, dt\, dV} \qquad (9)$$

As expected, the differential image exhibits an overall fourth-order nonlinearity, which can be regarded as two-photon ground-state depletion followed by two-photon probing.

Experimentally, we have demonstrated high-contrast imaging deep inside scattering samples by implementing such a two-photon induced focal saturation imaging technique for fluorescent beads imbedded in 3D scattering gels (Fig. 4c) and mouse kidney tissues (Fig. 4d). While this approach is conceptually appealing and experimentally simple, we point out that the practical limit is the deliverable high power needed for saturated excitation.

5. FUTURE PROSPECTS

We reported three super-nonlinear techniques here for high-contrast deep tissue imaging by harnessing three different spectroscopic transitions. MPAI utilizes special optical highlighters that can be switched between off- and on- states by external light, SERF adopts an additional laser to induce stimulated emission of the excited fluorophores, and two-photon induced focal saturation imaging relies on high power excitation to deplete the focal ground state fluorophores which can be then probed by two-photon fluorescence.

Comparing to conventional virtue-state mediated nonlinear imaging techniques (such as direct three-photon or four-photon excited fluorescence), our techniques are easy to implement and practically attractive for bio-imaging. First, the simultaneous three-photon (or four-photon) absorptions via virtual states are extremely improbable events (governed by fifth-order or seventh-order susceptibility) [17], while our super-nonlinearity is achieved by real-state-mediated sequential photon absorption, which can proceed with considerable efficiency. Second, the laser excitation wavelength in the direct three-photon or four-photon imaging for the classic GFP, YFP and RFP will need to be longer than 1400 nm, which lies outside the transparent optical window (650~1300nm) of most biological tissues. In contrast, our work still utilizes standard two-photon excitation wavelengths (~ 700-1000 nm) within the transparent optical window.

Finally, it is constructive to note that all the spectroscopic principles (i.e. PAFs, stimulated emission, and saturated excitation) adopted here have also played indispensable roles for breaking the diffraction-limited spatial resolution of fluorescence microscopy. In the well-known superresolution techniques, photoactivated localization microscopy (PALM) or stochastic optical reconstruction microscopy (STORM) utilizes photoactivation or photoswitching (18-20),

stimulated emission depletion microscopy (STED) employs stimulated emission (21) and nonlinear structured illumination microscopy adopts saturated excitation scheme (22). In essence, the coarse spatial resolution and the superficial penetration depth are both rooted in the difficulty of distinguishing identical molecules in space. By offering the additional disparity of molecular quantum states, spectroscopic transitions such as photoswitching, stimulated emission and focal saturation render the capability of circumventing both resolution and penetration limits.

REFERENCE:

(1) W. Denk, J. H. Strickler and W. W. Webb. "Two-photon laser scanning fluorescence microscopy," *Science* **248**(4951), 73–76 (1990).

(2) P. Theer, M. T. Hasan and W. Denk. "Two-photon imaging to a depth of 1000 μm in living brains by use of a Ti:Al_2O_3 regenerative amplifier," *Opt. Lett.* **28**(12), 1022–1024 (2003).

(3) P. Theer and W. Denk. "On the fundamental imaging-depth limit in two-photon microscopy," *J. Opt. Soc. Am. A*. **23**(12), 3139-3149(2006).

(4) N. Ji, D. E. Milkie, and E. Betzig, "Adaptive optics via pupil segmentation for high-resolution imaging in biological tissues," *Nat. Methods* **7**, 141-147 (2010).

(5) M. Rueckel, J. A. Mack-Bucher, and W. Denk, "Adaptive wavefront correction in two-photon microscopy using coherence-gated wavefront sensing," *Proc. Natl. Acad. Sci. USA* **103**, 17137-17142 (2006).

(6) M. A. A. Neil, R.Juskaitis, and T. Wilson, "Method of obtaining optical sectioning by using structured light in a conventional microscope," *Opt. Lett.* **22**, 1905-1907 (1997).

(7) D. Kobat, N. G. Horton, and C. Xu, "In vivo two-photon microscopy to 1.6-mm depth in mouse cortex," *J. Biomed. Opt.* **16**, 106014 (2011).

(8) Z. Yaqoob, D. Psaltis, M. S. Feld, and C. Yang, "Optical phase conjugation for turbidity suppression in biological samples," *Nature Photon.* **2**, 110-115 (2008).

(9) A. Leray, K. Lillis, and J. Mertz, "Enhanced background rejection in thick tissue with differential-aberration two-photon microscopy," *Biophys. J.* **94**, 1449-1458 (2008).

(10) N. Chen, C. H. Wong, and C. J.Sheppard, "Focal modulation microscopy," *Opt. Express* **16**, 18764-18769 (2008).

(11) Z. Chen, ***L. Wei***, X. Zhu and W. Min, "Extending the fundamental imaging-depth limit of multi-photon microscopy by imaging with photo-activatable fluorophores," *Opt. Express* 20, 18525 (2012).

(12) Y.-T. Kao, X. Zhu, F. Xu and W. Min, "Focal switching of photochromic fluorescent proteins enables multiphoton microscopy with superior image contrast," *Biomed. Opt. Express* 3, 1955 (2012).

(13) X. Zhu, Y.-T. Kao and W. Min, "Molecular-switch-mediated multiphoton fluorescence microscopy with high-order nonlinearity," *J. Phys. Chem. Lett.* 3, 2082 (2012).

(14) ***L. Wei***, Z. Chen and W. Min, "Stimulated emission reduced fluorescence microscopy: a concept for extending the fundamental depth limit of two-photon fluorescence imaging," *Biomed. Opt. Express* **3**, 1465 (2012).

(15) ***L. Wei*** and W. Min. "What can stimulated emission do for bio-imaging?" *Ann. N.Y. Acad. Sci.* **1293**, 1 (2013).

(16) ***L. Wei***, Z. Chen and W. Min. "Focal saturation and harmonic demodulation extend the fundamental imaging-depth limit of two-photon fluorescence microscopy," *In preparation.*

(17) N. G. Horton, et al. "In vivo three-photon microscopy of subcortical structures within an intact mouse brain." *Nat. Photonics.* **7**, 205-209 (2013).

(18) E. Betzig, et al, "Imaging intracellular fluorescent proteins at nanometer resolution," *Science* **313**, 1642-1645 (2006).

(19) S. T. Hess, T. P. K. Girirajan and M. D. Mason. "Ultra-igh resolution imaging by fluorescence photoactivation localization microscopy," *Biophys J*. **91**, 4258–4272 (2006).

(20) B. Huang, H. Babcock, and X. Zhuang, "Breaking the diffraction barrier: super-resolution imaging of cells," *Cell* **143**, 1047-1058 (2010).

(21) S. W. Hell, "Far-field optical nanoscopy," *Science* **316**, 1153-1158 (2007).

(22) M. G. L. Gustafsson, "Nonlinear structured-illumination microscopy: wide-field fluorescence imaging with theoretically unlimited resolution." *Proc. Natl. Acad. Sci. U.S.A.* **102**, 13081 (2005).